PAPER • OPEN ACCESS

Observation of orbital ordering and origin of the nematic order in FeSe

To cite this article: R X Cao *et al* 2019 *New J. Phys.* **21** 103033

New Journal of Physics
The open access journal at the forefront of physics

Deutsche Physikalische Gesellschaft DPG
IOP Institute of Physics

Published in partnership with: Deutsche Physikalische Gesellschaft and the Institute of Physics

OPEN ACCESS

RECEIVED
5 June 2019

REVISED
2 September 2019

ACCEPTED FOR PUBLICATION
30 September 2019

PUBLISHED
15 October 2019

PAPER

Observation of orbital ordering and origin of the nematic order in FeSe

R X Cao[1,2], Jian Hu[1], Jun Dong[1], J B Zhang[1], X S Ye[1], Y F Xu[1], D A Chareev[3,4,5], A N Vasiliev[6,7,8], Bing Wu[9], X H Zeng[1,11], Q L Wang[10,11] and Guoqing Wu[1,11]

[1] College of Physics Science and Technology, Yangzhou University, Yangzhou, Jiangsu 225002, People's Republic of China
[2] National Laboratory of Solid State Microstructures, Nanjing University, Nanjing 210093, People's Republic of China
[3] Institute of Experimental Mineralogy, Russian Academy of Sciences, 142432, Chernogolovka, Moscow District, Russia
[4] Institute of Physics and Technology, Ural Federal University, Mira st. 19, Ekaterinburg, 620002, Russia
[5] Kazan Federal University, 18 Kremlyovskaya Str., Kazan, 420008, Russia
[6] Low Temperature Physics and Superconductivity Department, Lomonosov Moscow State University, Moscow 119991, Russia
[7] National University of Science and Technology 'MISiS', Moscow 119049, Russia
[8] National Research South Ural State University, Chelyabinsk 454080, Russia
[9] Department of Math and Computer Science, Fayetteville State University, Fayetteville, NC 28301, United States of America
[10] Institute of Electrical Engineering, Chinese Academy of Sciences, Beijing 100190, People's Republic of China
[11] Authors to whom any correspondence should be addressed.

E-mail: xhzeng@yzu.edu.cn, qiuliang@mail.iee.ac.cn and wugq@yzu.edu.cn

Keywords: nuclear magnetic resonance (NMR), NMR spin-lattice relaxation, nematic order, orbital ordering, Fe-based superconductor

Abstract

In iron-based superconductors the interactions driving the nematic order that breaks the lattice four-fold rotational symmetry in the iron plane may also facilitate the Cooper pairing, but experimental determination of these interactions is challenging because the temperatures of the nematic order and the order of other electronic phases appear to match each other or to be close to each other. Here we performed field-dependent ^{77}Se-nuclear magnetic resonance (NMR) measurements on single crystals of iron-based superconductor FeSe, with magnetic field B_0 up to 16 T. The ^{77}Se-NMR spectra and Knight shift split when the direction of B_0 is away from the direction perpendicular to the iron planes (i.e. $B_0 \parallel c$) upon cooling in temperature, with a significant change in the distribution and magnitude of the internal magnetic field at the ^{77}Se nucleus, but these do not happen when B_0 is perpendicular to the iron planes, thus demonstrating that there is an orbital ordering. Moreover, stripe-type antiferromagnetism is absent, while giant antiferromagnetic spin fluctuations measured by the NMR spin-lattice relaxation gradually developed starting at ~40 K, which is far below the nematic order temperature $T_{\rm nem} = 89$ K. These results provide direct evidence of orbital-driven nematic order in FeSe.

1. Introduction

The interactions between structure, magnetism and superconductivity in Fe-based superconductors have been of wide interests [1–3]. The experimental determination of these interactions is challenging due to the occurrence of nematic order often at or near the temperature of a stripe-type long-range antiferromagnetic (AFM) order [4–8]. Similar to the stripe-type AFM order, the nematic order also breaks the lattice four-fold (C_4) rotational symmetry of a high-temperature phase, as evidenced by a tetragonal-to-orthorhombic structural phase transition at T_s [7–11]. On the other hand, the nematic order is directly linked to the superconducting state because nematic instability is a characteristic feature of the normal state upon which at lower temperatures the superconductivity emerges [1, 8, 12, 13], and thus nematicity is deemed a precursor of superconductivity in unconventional superconductors including the cuprates. It is generally believed that the nematic order is electronic and the structural phase transition is the consequence of the nematic order, since the lattice distortion is much smaller than the observed anisotropy of the in-plane resistivity in the nematic phase [9, 14]. However, it

remains highly controversial regarding the origin of the nematic order whether it is driven by spin order [15, 16], AFM spin fluctuations [15–17], and/or orbital order [18–24].

In Fe-based superconductors, FeSe has the simplest crystal structure, while it has representative properties as other Fe-based superconductors, thus it has been intensively studied [25–27]. FeSe undergoes a tetragonal-to-orthorhombic structural phase transition at $T_s \sim 90$ K with an electronic nematic order simultaneously ($T_{nem} = T_s$) [3, 28–30]. The orbital ordering was also found at T_{nem} via angle-resolved photoemission spectroscopy [29, 31, 32], whereas AFM order was absent at ambient pressure [28, 33, 34], and thus possible orbital order driven nematicity was proposed [3, 29, 31, 32].

However, recent findings show that stripe-type AFM order emerges under high pressure, and the AFM ordering temperature increases with high pressure [17, 33, 35–37]. These findings make the origin of the electronic nematic order more elusive. Even though various experimental techniques have been used for the study, most research work reported was focused on the doping and high pressure effects on the properties of FeSe. A systematical investigation of the effect of applied magnetic field on the properties of FeSe is still lacking.

Here we present for the first time field-dependent ^{77}Se-nuclear magnetic resonance (NMR) measurements systematically on high-quality single crystals of FeSe with applied magnetic field B_0 up to 16 T and temperature down to 1.5 K. We observed orbital ordering which is demonstrated by the splitting of the NMR spectrum and Knight shift. As measured by the ^{77}Se-NMR spin-lattice relaxation, giant AFM spin fluctuations gradually develop starting at ~40 K, which is far below the nematic order temperature $T_{nem} = T_s = 89$ K. These discoveries provide direct evidence of orbital-driven nematic order in FeSe. They also shed light on the important role of the nematic order on the superconductivity of Fe-based superconductors.

2. Experimental section

Single crystals of FeSe were grown in evacuated quartz ampoules using the $AlCl_3$/KCl flux technique with a temperature gradient of 5 °C cm^{-1} along the ampoule length. The temperatures of the hot and cold ends used for the growth were 427 °C and 380 °C, respectively. X-ray diffraction verified that the crystals have a high-purity single phase with a tetragonal crystal structure at room temperature, where the lattice c-axis is perpendicular to the Fe-planes (ab-plane). A SQUID magnetometer was used to measure the DC magnetic susceptibility $\chi(T)$. The sample used for our NMR measurements has a typical size of $3.3 \times 2.7 \times 0.1$ mm^3.

The NMR coil used for the measurements was made from 50 μm diameter silver wire wound with ~18 turns and attached to a goniometer on an NMR probe by epoxy. A single-crystal FeSe sample was put inside the coil so that the sample rotation axis is in the lattice ab-plane and perpendicular to the applied field B_0. A commercial network analyzer was used for the observation of the tuning and matching of the resonant circuit located at the bottom of the NMR probe. The NMR spectra and spin-lattice relaxation time T_1 were measured with an inversion-recovery method, where a π pulse is first applied to invert the nuclear magnetization M_0 to the $-z$ axis, and then after a delay time t, a $\pi/2$ pulse is applied to measure the recovering magnetization $M(t)$ component along the z axis, which gives T_1 as a function of time t as $M(t)/M_0 = 1 - 2\exp(-t/T_1)$ [38].

3. Results and discussion

Figure 1(a) shows the typical ^{77}Se-NMR spectra at $B_0 = 12$ T and temperature $T = 40$ K (below T_{nem}), by the variation of the angle θ between B_0 and the lattice c-axis of FeSe. The spectrum splits into two peaks (P_1 and P_2) which is observed when B_0 is applied ~25° from the c-axis. The splits reach the maximum when $B_0 \| a\&b$, indicating the largest anisotropy of the internal field at the Se-sites in the $a\&b$-plane.

Figure 1(b) exhibits the temperature (T) dependence of the ^{77}Se-NMR spectrum linewidth (Δf) at $B_0 \| c$ and $\| a\&b$, from the measurements of the temperature-dependent ^{77}Se-NMR spectra at $B_0 = 12$ T for both field directions. It shows a significant change at $B_0 \| a\&b$, but not at $B_0 \| c$.

Noticeably, the ^{77}Se-NMR spectra are fully magnetic with no electron charge or quadrupolar contributions because ^{77}Se is a spin $I = 1/2$ nucleus (which has no quadrupole moment). The spectral splitting was only observed when temperature T is less than $T_{nem} = T_s = 89$ K, but not for $B_0 \| c$ (the reason to be revealed later).

Thus, undoubtedly the spectrum split is the result of a structure symmetry break in the ab-plane due to the tetragonal-to-orthorhombic structure phase transition (structurally a and b are not equal any more), which is known as the consequence of the electronic nematic order in the Fe-planes [23, 24].

Moreover, with the nematic order the spectrum splits also reflect a significant change in spacial field distribution (ΔB_{FWHM}) and also a change in the value of the internal field (B') at the Se-sites. Here $\Delta B_{FWHM} = \Delta f / {}^{77}\gamma_I$, where ${}^{77}\gamma_I = 8.131$ MHz/T is the gyromagnetic ratio of the ^{77}Se nucleus, and $B' = (\nu - \nu_L)/{}^{77}\gamma_I$, where ν is the NMR frequency and ν_L is the Larmor frequency ($\nu_L = {}^{77}\gamma_I B_0$).

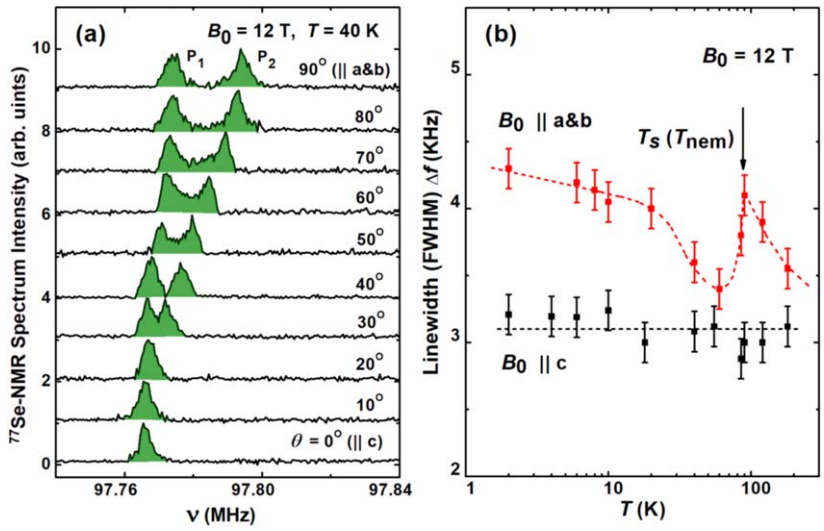

Figure 1. (a) ^{77}Se-NMR spectra of FeSe measured at $B_0 = 12$ T and $T = 40$ K as a function of angle θ, where θ is the angle between B_0 and the lattice c-axis. (b) T-dependence of the ^{77}Se-NMR linewidth (FWHM) Δf at $B_0 \| a\&b$ and $B_0 \| c$. The dashed lines are guides to the eyes.

For example, above T_{nem} the linewidth $\Delta f = 3.5$ kHz at $T = 200$ K. Upon cooling in temperature, it goes up and it reaches a maximum of 4.2 kHz at $T = T_{nem}$ (figure 1(b)), followed by a complete separation of the two NMR spectrum peaks, and $\Delta f = 3.5$ kHz at $T \sim 60$ K again. Then Δf increases upon further cooling. While the spectrum linewidth Δf(FWHM) at $B_0 \parallel c$ keeps no change down to low T (figure 1(b)).

At the meantime, the value of the internal field B' at the Se-sites has a change $\Delta B' = \pm 12.0$ G (a Knight shift change of $\pm 0.010\%$) from the average value ($\overline{B'}$) of the internal field $\overline{B'} = 160$ G (or an average Knight shift 0.133%) (not shown here), i.e. the change of the value of internal field $\Delta B'$ reaches $\pm 7.5\%$ from the average value of the internal field $\overline{B'}$ in the Fe-planes.

The Knight shift K is defined by $K = (\nu - \nu_L)/\nu_L$ as a tradition, and it should be field independent. That the values of $K(T)$ at $B_0 \| a\&b$ are apparently larger than those at $B_0 \| c$ at $T < T_{nem}$ indicates an anisotropic hyperfine coupling.

In general, the Knight shift K is given by [39, 40]:

$$K = K_{spin} + K_{orb}, \tag{1}$$

where spin Knight shift $K_{spin} = [A_{spin}/N_A\mu_B]\chi_{spin}$, and orbital Knight shift $K_{orb} = [A_{orb}/N_A\mu_B]\chi_{orb}$. Here χ_{spin} and χ_{orb} are the electron spin and orbital susceptibility, respectively. A_{spin} and A_{orb} are the hyperfine coupling constants between the studied nucleus and the electron spins and the electron orbitals, respectively. N_A is the Avogadro's number and μ_B is the Bohr magneton. Likewise, the magnetic susceptibility χ is the sum of the contributions from core diamagnetic susceptibility (χ_{dia}), orbital (van Vleck) paramagnetic susceptibility (χ_{orb}) and Pauli spin paramagnetic susceptibility (χ_{spin}) [41, 42], i.e. $\chi = \chi_{dia} + \chi_{orb} + \chi_{spin}$. Here, for FeSe, $\chi_{dia} = -6.1 \times 10^{-5}$ cm^3/mol from the diamagnetism of the atomic ions, and χ_{orb} is T-independent unless there is an orbital change such as an orbital ordering.

Figure 2(a) exhibits the relation of the Knight shift $K(T)$ with the sample susceptibility $\chi(T)$, plotted as $K(T)$ versus $\chi(T)$. At $T \geqslant T_{nem}$, $K(T)$ is linear with $\chi(T)$ as expected from above, from which we obtain the value of the constant of the hyperfine coupling to the electron spins at $B_0 \| a\&b$: $A_{spin,\|a\&b} = 30.4$ kOe/μ_B, and similarly the corresponding hyperfine coupling constant at $B_0 \| c$: $A_{spin,\|c} = 32.8$ kOe/μ_B. As discussed later, the constants (A_{orb}) of the hyperfine coupling to the electron orbitals are also obtained, the values of the spin Knight shift K_{spin} and orbital shift K_{orb} are separated, and χ_{orb} and $\chi_{spin}(T)$ are distinguishable, both at $B_0 \| a\&b$ and at $B_0 \| c$.

Interestingly, at $T < T_{nem}$, $K(T)$ versus $\chi(T)$ gradually deviates from the high temperature linear relation, as seen in figure 2(a) for both $B_0 \| a\&b$ and $B_0 \| c$. Because $K(T)$ and $\chi(T)$ are fully magnetic in nature, as described by equation (1), this deviation can only be explained by a change in the electron spin susceptibility $\chi_{spin}(T)$ such as that as a result of an AFM order of the electron spins or AFM spin fluctuations, and/or by a change in the electron orbital susceptibility χ_{orb} such as that as a result of an ordering of the electron orbitals, as well as associated changes in the hyperfine couplings to the electron spins (A_{spin}) and/or to the electron orbitals (A_{orb}), any of which could lead to a change in $K(T)$ simultaneously. This is also seen by the expression [39, 40, 42]

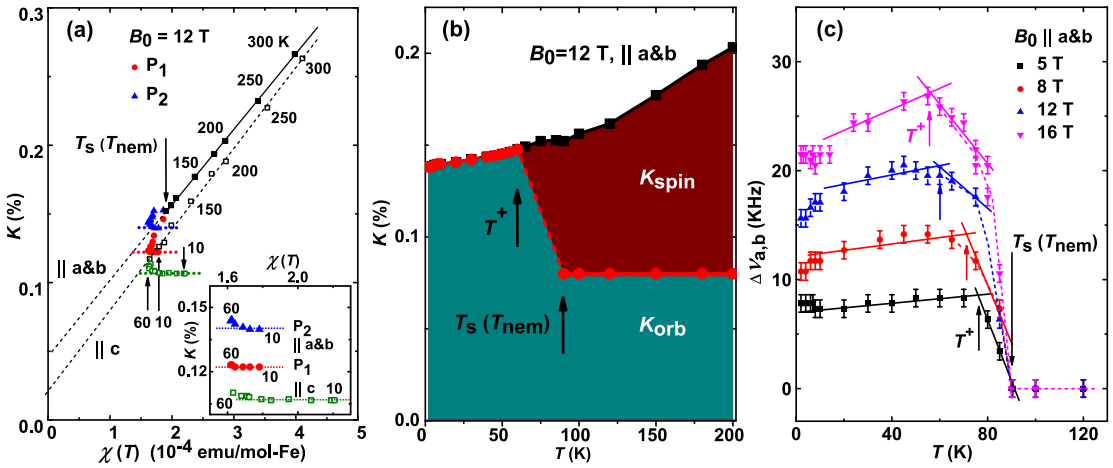

Figure 2. (a) Knight shift $K(T)$ versus magnetic susceptibility $\chi(T)$ plot, where the straight lines are for the slopes above T_{nem}. The inset of (a) is an enlargement for the data at $T = 60$–10 K (note: the critical temperature of superconductivity $T_c < 10$ K). (b) ^{77}Se-NMR Knight shift $K(T)$ versus T including the contributions of the spin Knight shift K_{spin} and orbital Knight shift K_{orb} when $B_0 \| a\&b$-plane. (c) Field-dependence of the difference of the in-plane NMR spectrum peak frequency ($\Delta\nu_{a,b}$) upon cooling in temperature. The dashed lines in (c) are guides to the eyes and the solid lines in (c) are the fit to determine T^+.

$$K(T) = K_{spin}(T) + K_{orb} = \frac{A_{spin}}{N_A \mu_B}\chi_{spin}(T) + \frac{A_{orb}}{N_A \mu_B}\chi_{orb}$$
$$= \frac{A_{spin}}{N_A \mu_B}[\chi(T) - \chi_{orb} - \chi_{dia}] + \frac{A_{orb}}{N_A \mu_B}\chi_{orb}, \quad (2)$$

where only $K(T)$ and $\chi(T)$ are temperature dependent.

However, surprisingly, upon further cooling in temperature, the $K(T)$–$\chi(T)$ plot exhibited in figure 2(a) inset shows that the slope of $K(T)$ versus $\chi(T)$ is ~0, both at $B_0 \| a\&b$ and $B_0 \| c$ at $B_0 = 12$ T in the temperature range ~60−10 K, which is a wide range of temperature below T_{nem} and above the critical temperature T_c of superconductivity, i.e. $K_{spin,\|a} \approx 0$, $K_{spin,\|b} \approx 0$, and $K_{spin,\|c} \approx 0$. This is also true for all other fields we applied. That is to say that below T_{nem} the spin Knight shift $K_{spin}(T)$ becomes negligible at all directions, i.e. $K \approx K_{orb}$.

In other words, the Knight shift $K(T)$ at low temperatures predominantly comes from the contribution of the orbital Knight shift K_{orb} (figure 2(b)).

The reason that $K_{spin}(T) \approx 0$ in all directions can be understood by enormous AFM spin fluctuations developed in the same temperature regime, whereas there is no existence of electron spin order, as directly evidenced by our ^{77}Se-NMR spin-lattice relaxation data (see next), with the consideration of a more general expression of the spin Knight shift as [39, 42]: $K_{spin} = \sum_i \frac{A^i_{spin}}{N_A \mu_B}\chi^i_{spin}(T)$. This is the summation of the terms of hyperfine coupling interaction to the individual electron spins (the degree of electron spin polarization is $\propto \chi^i_{spin}$), where each term could be very different from each other due to the AFM spin fluctuations, resulting in a cancellation of them.

On the other hand, the dramatic increase of the orbital Knight shift K_{orb} (figure 2(b)) below T_S (T_{nem}) must be the result of an orbital ordering. To confirm this, we studied the internal field difference ($\Delta B'_{a,b}$) in the ab-plane by the measurement of the frequency difference ($\Delta\nu_{a,b}$) of the NMR spectrum peaks (P_1 and P_2), as shown in figure 2(c). $\Delta\nu_{a,b}$ reaches ~12.5 kHz and 25.0 kHz, or a value of internal field difference $\Delta B'_{a,b} \approx 15.6$ G and 31.2 G at $B_0 = 8$ T and 16 T, respectively, at low temperatures. These values are scalable with B_0, which is understandable as they are magnetic in nature. Here we have $\Delta B'_{a,b} = \Delta\nu_{a,b} / {}^{77}\gamma_{Se}$. Since there is no appearance of AFM spin order and the in-plane anisotropy of the paramagnetic spin Knight shift is expected to be negligible (i.e. $K_{spin,\|a} \approx K_{spin,\|b}$), from the Knight shift we have

$$\Delta B'_{a,b} = B_0[(K_{spin,\|a} - K_{spin,\|b}) + (K_{orb,\|a} - K_{orb,\|b})] \approx B_0(K_{orb,\|a} - K_{orb,\|b}). \quad (3)$$

Therefore, this indicates that all the data values of $\Delta\nu_{a,b}$ shown in figure 2(c), are essentially completely from the orbital contributions (for convenience, we say all orbital), i.e. the internal field difference in the ab-plane is fully determined by the difference of the hyperfine coupling to the Fe-electron orbitals among the a-and b-axes. In other words, these data verify that there is an electron orbital ordering occurring at $T \leqslant T_{nem}$.

Now we can define a characteristic orbital ordering temperature T^+ by the intersection of two lines that fit to the data in the transition area as shown in figure 2(c), and we find that T^+ is linear to B_0 as: $T^+ = T_{nem} - kB_0$, where $k = 2.4 \pm 0.1$ (K/T) (figure 4). We noted that T^+ indicates the temperature where orbital ordering is

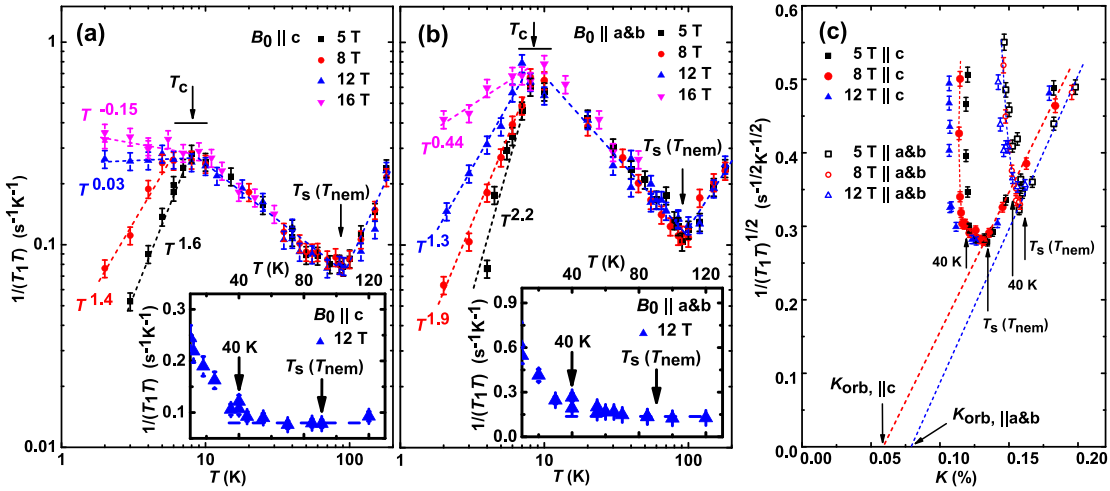

Figure 3. Field-dependence of the ^{77}Se-NMR spin-lattice relaxation in FeSe upon cooling in temperature (T). ^{77}Se $1/T_1T$ versus T at (a) $B_0 \| c$ and (b) $B_0 \| a\&b$, respectively. The insets are enlargements in the low T regime. (c) Plot of $\sqrt{1/(T_1T)}$ versus Knight shift $K(T)$, where the straight dashed lines are the fits to the Korringa law (equation (4)).

fully developed while the orbital ordering starts at $T_{\rm nem}$ upon cooling. Here $\Delta\nu_{a,b}$ or $\Delta B'_{a,b}$ can be treated as the orbital ordering parameter [23], $\Delta\nu_{a,b} \propto \sqrt{T_{\rm nem} - T}$ near $T = T_{\rm nem}$, and as $B_0 \to 0$, $T^+ = T_{\rm nem}$.

Furthermore, in order to investigate the electron spin dynamics and to support the observations in the NMR spectrum and Knight shift, we performed the ^{77}Se-NMR spin-lattice relaxation measurements as a function of temperature and applied field, as exhibited in figure 3.

Generally, $1/T_1T$ probes the imaginary part of the low-frequency ($\omega \to 0$) dynamical susceptibility [$\chi(q, \omega)$] averaged over the momentum (q) space as [39, 43]: $1/T_1T = [3k_{\rm B}/(4\mu_{\rm B}^2\hbar^2)]\sum_q A_q A_{-a}\chi''(q, \omega)/\omega$, where A_q is the hyperfine coupling constant. For conventional Fermi liquid conductors, $\sum_a \chi''(q, \omega) = \pi\sum_{k,k'} \delta(E_k - E_{k'} - \hbar\omega) f(E_k - E_{k'})$, which gives the Korringa law [39, 43]:

$$\begin{aligned} 1/T_1T &= (\pi/\hbar)A_{hf}^2 N^2(E_{\rm F}) k_{\rm B} \\ &= (4\pi k_{\rm B}/\hbar)(\gamma_I/\gamma_e)^2 K_{\rm spin}^2, \end{aligned} \tag{4}$$

where $\gamma_{I(e)}$ is the gyromagnetic ratio of nucleus (electron), $N(E_{\rm F})$ is the density of states of electrons at the Fermi energy $E_{\rm F}$, and $f(E)$ is the energy distribution function. For AFM correlated electrons, $\chi(q)$ can have a peak at the AFM wave factor $Q = (\pi, \pi)$, and then $1/T_1T \propto \chi(Q)$ with a Curie–Weiss type relation as: $1/T_1T = C'/(T - \theta)$, as often seen in cuprate and other Fe-based superconductors [6, 44–46]. For AFM fluctuations, the fit parameter $\theta < 0$, and for large spin fluctuations C' is large.

Thus, important information can be obtained from the NMR spin-lattice relaxation. First, figures 3(a) and (b) show the nematic order/structure phase transition at $T_{\rm nem} = T_{\rm s}$, which is independent of B_0. Second, enormous AFM spin fluctuations are developed (a significant deviation from the Korringa law) as seen in the plot of $\sqrt{1/(T_1T)}$ versus T but they start at ~40 K and below only (inset of figures 3(a) and (b)), which is far below $T_{\rm nem} = 89$ K. With the fit to the Curie–Weiss relation for 10 K $< T <$ 40 K, we have the values of $\theta = -4.6\,(-21.5)$ K, and $C' = 10.0\,(7.2)\,{\rm s}^{-1}$ for $B_0 \| a\&b\,(B_0 \| c)$. Here θ is comparable while C' is much larger than those of other Fe-based superconductors [47–50]. Third, the AFM spin fluctuations drop significantly at $T < T_{\rm c}$ due to diamagnetism associated with the pairing symmetry of the electron spins, and $1/T_1 \propto T^{\alpha}$, where $\alpha \approx 3$ in low fields, consistent with a line-node gap behavior of a d-wave superconductor, agreeing with reports on various Fe-based superconductors [35, 40, 47, 51].

Figure 3(c) exhibits the plot of $\sqrt{1/(T_1T)}$ versus $K(T)$ with T as an implicit parameter, with the consideration that the Korringa law (equation (4)) can also be expressed as $\sqrt{1/(T_1T)} = \sqrt{C}\,K_{\rm spin}(T) = \sqrt{C}\,[K(T) - K_{\rm orb}]$ for a Fermi liquid. Here $C = (4\pi k_{\rm B}/\hbar)(\gamma_I/\gamma_e)^2$ for free electrons [39, 43]. Apparently, figure 3(c) shows a linear relation above $T_{\rm nem}$, and thus it gives values of $K_{\rm orb} \approx 0.06\%$ (0.08%) for $B_0 \| c\,(B_0 \| a\&b)$ by the intercepts along the $K(T)$ axis, which have been used to separate $K_{\rm spin}$ and $K_{\rm orb}$ in the tetragonal phase (shown in figure 2(b)) and to extrapolate the values of $A_{\rm orb}$, $A_{\rm spin}$, $\chi_{\rm orb}$, and $\chi_s(T)$ combining with the $K(T) - \chi(T)$ relation (figure 3(c)). Similarly, the slope also gives an experimental value of $C \approx 1.5 \times 10^5\,(1.8 \times 10^5)\,{\rm K}^{-1}\,{\rm s}^{-1}$ for $B_0 \| c\,(B_0 \| a\&b)$, which matches well with the theoretical value of $C = 1.46 \times 10^5\,{\rm K}^{-1}\,{\rm s}^{-1}$ for non-interacting/free electrons in FeSe. Thus, these data verify that the electrons at $T > T_{\rm nem}$ in FeSe are not strongly correlated.

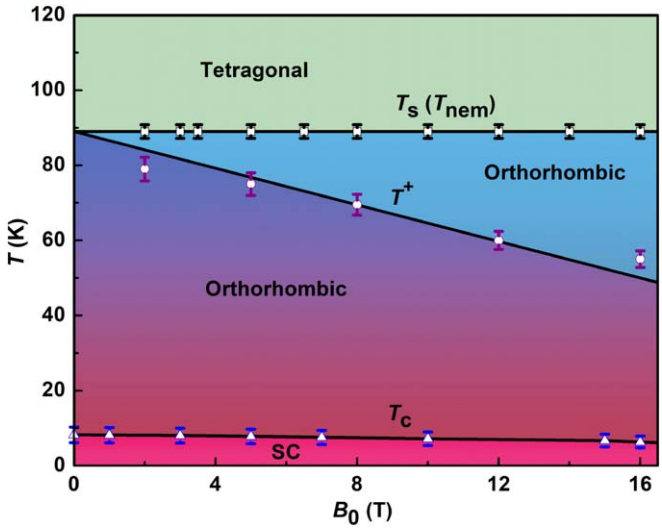

Figure 4. The temperature-field (T–B_0) phase diagram of FeSe. The obtained phase diagram of FeSe in applied magnetic field B_0 with temperatures T_s, T_{nem}, T^+, and T_c (see text for definition). The solid lines are guides to the eyes.

Moreover, below T_{nem} in the range 40 K $< T \leqslant T_{nem}$, $1/T_1T$ continues to show a free-electron behavior (Korringa law), where $1/T_1T$ is a constant as exhibited in figures 3(a), (b) insets, i.e. there is essentially no AFM spin fluctuations at the T_{nem} regime over a wide range of temperature. Therefore, AFM spin fluctuations can be excluded from the driving mechanism of the nematic order.

Figure 4 shows temperature—field phase diagram we obtained. First, as described in detail above, the applied magnetic field decreases the characteristic orbital ordering temperature T^+ rather sensitively. Second, the structural phase transition temperature T_s and the nematic ordering temperature T_{nem} are not affected by the applied field ($T_{nem} = T_s = 89$ K). Third, stripe-type AFM order is absent at all the applied fields. Here the values of T_c were determined by our resonance frequency method [52].

We would like to point out that, among the two groups of the 3d Fe t_{2g} (d_{xy}, d_{yz}, d_{xz}) and e_g ($d_{x^2-y^2}$, $d_{3z^2-r^2}$) orbitals (totally five orbitals), d_{xy}, $d_{x^2-y^2}$, and $d_{3z^2-r^2}$ are rotationally symmetric in the xy-plane. Thus, the only two candidates related to the tetragonal-orthorhombic degeneracy (lattice symmetry breaking) are the d_{yz} and d_{xz} orbitals. And, what an NMR spectrum directly measures is the local field distribution and local field values parallel to the externally applied magnetic field at the nucleus at the atomic scale. Therefore, because of the unique symmetry of the d_{yz} and d_{xz} orbitals in the lattice axis c-direction the ordering of these d_{yz} and d_{xz} orbitals is not able to cause any splitting of the ^{77}Se-NMR spectra at $B_0 \| c$ in FeSe.

Finally, we discuss the field effect on the characteristic temperatures. That the values of T_s (T_{nem}) are not affected by the directions or magnitude of the applied field could be explained by the weak anisotropy character of the paramagnetic Fe-spins in the high symmetry tetragonal lattice. That T^+ is linearly proportional to B_0 could be understood due to its full magnetic character that involves electron orbital moments, while the reason for the decrease of the value of T^+ with B_0 is not clear.

Whereas there is no appearance of long-range AFM order of the electron spins, we note that there were reports about short-range stripe magnetic order and possible spin–orbital coupling [53–55] developing in the nematic phase. From our data of the temperature- and field-dependence of ^{77}Se-NMR spin-lattice relaxation, $1/T_1T$ versus T, we clearly see that giant AFM fluctuations gradually develop starting at ~40 K and below, which is far below the nematic order temperature T_{nem}. And above T_{nem} the data of $1/T_1T$ well follows the Korringa law, which is a direct evidence of trivial electron correlations. These results leave the orbital ordering unequivocally as the dominant driving force of the nematic order.

4. Conclusions

In summary, we report direct observation of orbital ordering which is demonstrated by the splitting of the ^{77}Se-NMR spectrum and Knight shift in single crystals of iron-based superconductor FeSe. As illustrated by the field-dependence of the ^{77}Se-NMR spin-lattice relaxation, stripe-type AFM order is absent, whereas giant AFM spin fluctuations developed starting at temperatures far below the electronic nematic order temperature T_{nem}, thus both of which can be unambiguously excluded from the origin of the nematic order. These discoveries provide direct evidence of orbital-driven nematic order in FeSe. Our results also help to the understanding of the

strong interplay between structure, magnetism and superconductivity in Fe-based superconductors as well as other unconventional superconductors.

Acknowledgments

Work at YZU was supported by National Science Foundation of China (NSFC) (Grants # 61474096 and 1804291) and NSF of Jiangsu (Grants # BK20180889 and BK20180890), and at CAS by NSFC (Grants # 51477167 and 41527802). DAC thanks supports by the program 211 of the Russian Federation Government (RFG), agreement 02.A03.21.0006 and by the RFG Program of Competitive Growth of KFU. ANV thanks supports by Russian Foundation for Basic Research Grant # 17-29-10007, by the Ministry of Education and Science of the RFG in the framework of ICP of NUST MISiS (Grant # K2-2017-084), and by Act 211 of RFG, agreements 02.A03.21.0004, 02.A03.21.0006, and 02.A03.21.0011.

ORCID iDs

X H Zeng https://orcid.org/0000-0003-4775-6764
Guoqing Wu https://orcid.org/0000-0003-1180-7208

References

[1] Paglione J and Greene R L 2010 High-temperature superconductivity in iron-based materials *Nat. Phys.* **6** 645
[2] Fernandes R M, VanBebber L H, Bhattacharya S, Chandra P, Keppens V, Mandrus D, McGuire M A, Sales B C, Sefat A S and Schmalian J 2010 Effects of nematic fluctuations on the elastic properties of iron arsenide superconductors *Phys. Rev. Lett.* **105** 157003
[3] Tanatar M A *et al* 2016 Origin of the resistivity anisotropy in the nematic phase of FeSe *Phys. Rev. Lett.* **117** 127001
[4] Kontani H, Saito T and Onari S 2011 Origin of orthorhombic transition, magnetic transition, and shear-modulus softening in iron pnictide superconductors: analysis based on the orbital fluctuations theory *Phys. Rev.* B **84** 024528
[5] Fernandes R M, Böhmer A E, Meingast C and Schmalian J 2013 Scaling between magnetic and lattice fluctuations in iron pnictide superconductors *Phys. Rev. Lett.* **111** 137001
[6] Nakai Y, Iye T, Kitagawa S, Ishida K, Kasahara S, Shibauchi T, Matsuda Y, Ikeda H and Terashima T 2013 Normal-state spin dynamics in the iron-pnictide superconductors Ba Fe_2 $(As_{1-x}$ $P_x)$ $_2$ and Ba $(Fe_{1-x}$ $Co_x)$ $_2$ As_2 probed with NMR measurements *Phys. Rev.* B **87** 174507
[7] Böhmer A E, Hardy F, Eilers F, Ernst D, Adelmann P, Schweiss P, Wolf T and Meingast C 2013 Lack of coupling between superconductivity and orthorhombic distortion in stoichiometric single-crystalline FeSe *Phys. Rev.* B **87** 180505(R)
[8] Fernandes R M, Chubukov A V and Schmalian J 2014 What drives nematic order in iron-based superconductors? *Nat. Phys.* **10** 97
[9] Chu J H, Analytis J G, De Greve K, McMahon P L, Islam Z, Yamamoto Y and Fisher I R 2010 In-plane resistivity anisotropy in an underdoped iron arsenide superconductor *Science* **329** 824–6
[10] Konstantinova T *et al* 2019 Photoinduced dynamics of nematic order parameter in FeSe *Phys. Rev.* B **99** 180102(R)
[11] Chen G Y, Wang E, Zhu X and Wen H H 2019 Synergy and competition between superconductivity and antiferromagnetism in FeSe under pressure *Phys. Rev.* B **99** 054517
[12] Kang J, Fernandes R M and Chubukov A 2018 Superconductivity in FeSe: the role of nematic order *Phys. Rev. Lett.* **120** 267001
[13] Liu D *et al* 2018 Orbital origin of extremely anisotropic superconducting gap in nematic phase of FeSe superconductor *Phys. Rev.* X **8** 031033
[14] Tanatar M A *et al* 2010 Uniaxial-strain mechanical detwinning of $CaFe_2As_2$ and $BaFe_2As_2$ crystals: optical and transport study *Phys. Rev.* B **81** 184508
[15] Fang C, Yao H, Tsai W F, Hu J and Kivelson S A 2008 Theory of electron nematic order in LaFeAsO *Phys. Rev.* B **77** 224509
[16] Hu J and Xu C 2012 Nematic orders in iron-based superconductors *Physica* C **481** 215–22
[17] Wang P S, Sun S S, Cui Y, Song W H, Li T R, Yu R, Lei H and Yu W 2016 Pressure induced stripe-order antiferromagnetism and first-order phase transition in FeSe *Phys. Rev. Lett.* **117** 237001
[18] Lv W, Wu J and Phillips P 2009 Orbital ordering induces structural phase transition and the resistivity anomaly in iron pnictides *Phys. Rev.* B **80** 224506
[19] Lee C C, Yin W G and Ku W 2009 Ferro-orbital order and strong magnetic anisotropy in the parent compounds of iron-pnictide superconductors *Phys. Rev. Lett.* **103** 267001
[20] Krüger F, Kumar S, Zaanen J and van den Brink J 2009 Spin–orbital frustrations and anomalous metallic state in iron-pnictide superconductors *Phys. Rev.* B **79** 054504
[21] Daghofer M, Luo Q L, Yu R, Yao D X, Moreo A and Dagotto E 2010 Orbital-weight redistribution triggered by spin order in the pnictides *Phys. Rev.* B **81** 180514
[22] Chen C C, Maciejko J, Sorini A P, Moritz B, Singh R R P and Devereaux T P 2010 Orbital order and spontaneous orthorhombicity in iron pnictides *Phys. Rev.* B **82** 100504
[23] Baek S H, Efremov D V, Ok J M, Kim J S, van den Brink J and Büchner B 2015 Orbital-driven nematicity in FeSe *Nat. Mater.* **14** 210
[24] Böhmer A E, Arai T, Hardy F, Hattori T, Iye T, Wolf T, v Löhneysen H, Ishida K and Meingast C 2015 Origin of the tetragonal-to-orthorhombic phase transition in FeSe: a combined thermodynamic and NMR study of nematicity *Phys. Rev. Lett.* **114** 027001
[25] Hsu F C *et al* 2008 Superconductivity in the PbO-type structure α-FeSe *Proc. Natl Acad. Sci.* **105** 14262–4
[26] Büchner B and Hess C 2009 Iron-based superconductors: vital clues from a basic compound *Nat. Mater.* **8** 615
[27] Stewart G R 2011 Superconductivity in iron compounds *Rev. Mod. Phys.* **83** 1589–652
[28] McQueen T M, Williams A J, Stephens P W, Tao J, Zhu Y, Ksenofontov V, Casper F, Felser C and Cava R J 2009 Tetragonal-to-orthorhombic structural phase transition at 90 K in the superconductor $Fe_{1.01}Se$ *Phys. Rev. Lett.* **103** 057002

[29] Nakayama K, Miyata Y, Phan G N, Sato T, Tanabe Y, Urata T, Tanigaki K and Takahashi T 2014 Reconstruction of band structure induced by electronic nematicity in an FeSe superconductor *Phys. Rev. Lett.* **113** 237001
[30] Shimojima T *et al* 2014 Lifting of *xz*/*yz* orbital degeneracy at the structural transition in detwinned FeSe *Phys. Rev.* B **90** 121111
[31] Watson M D *et al* 2015 Emergence of the nematic electronic state in FeSe *Phys. Rev.* B **91** 155106
[32] Zhang P *et al* 2015 Observation of two distinct d_{xz}/d_{yz} band splittings in FeSe *Phys. Rev.* B **91** 214503
[33] Bendele M, Amato A, Conder K, Elender M, Keller H, Klauss H H, Luetkens H, Pomjakushina E, Raselli A and Khasanov R 2010 Pressure induced static magnetic order in superconducting $FeSe_{1-x}$ *Phys. Rev. Lett.* **104** 087003
[34] Mizuguchi Y, Furubayashi T, Deguchi K, Tsuda S, Yamaguchi T and Takano Y 2010 Mössbauer studies on FeSe and FeTe *Physica* C **470** S338–9
[35] Imai T, Ahilan K, Ning F L, McQueen T M and Cava R J 2009 Why does undoped FeSe become a high-T_c superconductor under pressure? *Phys. Rev. Lett.* **102** 177005
[36] Sun J P *et al* 2016 Dome-shaped magnetic order competing with high-temperature superconductivity at high pressures in FeSe *Nat. Commun.* **7** 12146
[37] Kothapalli K *et al* 2016 Strong cooperative coupling of pressure-induced magnetic order and nematicity in FeSe *Nat. Commun.* **7** 12728
[38] Fukushima E and Roeder S B W 1981 *Experimental Pulse NMR: a Nuts and Bolts Approach* (Reading, MA: Addison-Wesley)
[39] Slichter C P 1989 *Principles of Magnetic Resonance* 3rd edn (Berlin: Springer)
[40] Kotegawa H, Masaki S, Awai Y, Tou H, Mizuguchi Y and Takano Y 2008 Evidence for unconventional superconductivity in arsenic-free iron-based superconductor FeSe: a ^{77}Se-NMR study *J. Phys. Soc. Jpn.* **77** 113703
[41] Kittel C 2005 *Introduction to Solid State Physics* 8th edn (New York: Wiley)
[42] Imai T, Ahilan K, Ning F, McGuire M A, Sefat A S, Jin R, Sales B C and Mandrus D 2008 NMR measurements of intrinsic spin susceptibility in $LaFeAsO_{0.9}$ $F_{0.1}$ *J. Phys. Soc. Jpn.* **77** 47–53
[43] Moriya T 1963 The effect of electron-electron interaction on the nuclear spin relaxation in metals *J. Phys. Soc. Jpn.* **18** 516–20
[44] Millis A J, Monien H and Pines D 1990 Phenomenological model of nuclear relaxation in the normal state of $YBa_2Cu_3O_7$ *Phys. Rev.* B **42** 167–78
[45] Aharen T *et al* 2010 Magnetic properties of the geometrically frustrated $s = \frac{1}{2}$ antiferromagnets, La_2LiMoO_6 and Ba_2YMoO_6, with the B-site ordered double perovskite structure: evidence for a collective spin-singlet ground state *Phys. Rev.* B **81** 224409
[46] Dai P 2015 Antiferromagnetic order and spin dynamics in iron-based superconductors *Rev. Mod. Phys.* **87** 855–96
[47] Nakai Y, Ishida K, Kamihara Y, Hirano M and Hosono H 2008 Evolution from itinerant antiferromagnet to unconventional superconductor with fluorine doping in LaFeAs (O_{1-x} F_x) revealed by ^{75}As and ^{139}La nuclear magnetic resonance *J. Phys. Soc. Jpn.* **77** 073701
[48] Ning F L, Ahilan K, Imai T, Sefat A S, McGuire M A, Sales B C, Mandrus D, Cheng P, Shen B and Wen H H 2010 Contrasting spin dynamics between underdoped and overdoped $Ba(Fe_{1-x}Co_x)_2As_2$ *Phys. Rev. Lett.* **104** 037001
[49] Kitagawa S, Nakai Y, Iye T, Ishida K, Kamihara Y, Hirano M and Hosono H 2010 Stripe antiferromagnetic correlations in $LaFeAsO_{1-x}F_x$ probed by ^{75}As NMR *Phys. Rev.* B **81** 212502
[50] Ma L, Chen G F, Yao D X, Zhang J, Zhang S, Xia T L and Yu W 2011 ^{23}Na and ^{75}As NMR study of antiferromagnetism and spin fluctuations in NaFeAs single crystals *Phys. Rev.* B **83** 132501
[51] Ning F, Ahilan K, Imai T, Sefat A S, Jin R, McGuire M A, Sales B C and Mandrus D 2008 ^{59}Co and ^{75}As NMR investigation of electron-doped high T_c superconductor $BaFe_{1.8}$ $Co_{0.2}$ As_2 ($T_c = 22$ K) *J. Phys. Soc. Jpn.* **77** 103705
[52] Cao R X, Dong J, Wang Q L, Yang Y J, Zhao C, Chareev D A, Vasiliev A N, Wu B, Wu G and Zeng X H 2019 Measurements of the superconducting anisotropy in FeSe with a resonance frequency technique *AIP Adv.* **9** 045220
[53] Ma M, Bourges P, Sidis Y, Xu Y, Li S, Hu B, Li J, Wang F and Li Y 2017 Prominent role of spin–orbit coupling in fese revealed by inelastic neutron scattering *Phys. Rev.* X **7** 021025
[54] Day R P *et al* 2018 Influence of spin–orbit coupling in iron-based superconductors *Phys. Rev. Lett.* **121** 076401
[55] He M, Wang L, Hardy F, Xu L, Wolf T, Adelmann P and Meingast C 2018 Evidence for short-range magnetic order in the nematic phase of FeSe from anisotropic in-plane magnetostriction and susceptibility measurement *Phys. Rev.* B **97** 104107